ECS Journal of Solid State
Science and Technology

OPEN ACCESS

Operation of NiO/β-$(Al_{0.21}Ga_{0.79})_2O_3$/$Ga_2O_3$ Heterojunction Lateral Rectifiers at up to 225 °C

To cite this article: Hsiao-Hsuan Wan *et al* 2023 *ECS J. Solid State Sci. Technol.* **12** 075008

ECS Journal of Solid State Science and Technology, 2023 12 075008

Operation of NiO/β-$(Al_{0.21}Ga_{0.79})_2O_3$/$Ga_2O_3$ Heterojunction Lateral Rectifiers at up to 225 °C

Hsiao-Hsuan Wan,[1,*,z] Jian-Sian Li,[1] Chao-Ching Chiang,[1,*] Xinyi Xia,[1] Fan Ren,[1,**] Hannah N. Masten,[2] James Spencer Lundh,[2] Joseph A. Spencer,[3,4] Fikadu Alema,[5] Andrei Osinsky,[5] Alan G. Jacobs,[3] Karl Hobart,[3] Marko J. Tadjer,[3] and S. J. Pearton[6,**]

[1]Department of Chemical Engineering, University of Florida, Gainesville, FL, 32611, United States of America
[2]National Research Council Postdoctoral Fellow at U.S. Naval Research Laboratory, United States of America
[3]U.S. Naval Research Laboratory, Washington, DC, United States of America
[4]Virginia Tech, Blacksburg Virginia, VA, United States of America
[5]Agnitron Technology, Inc., Chanhassen, MN, United States of America
[6]Department of Materials Science and Engineering, University of Florida, Gainesville, FL, 32611, United States of America

The characteristics of NiO/β-(Al0.21Ga0.79)2O3/Ga2O3 heterojunction lateral geometry rectifiers with the epitaxial layers grown by metal organic chemical vapor deposition were measured over a temperature range from 25 °C–225 °C. The forward current increased with temperature, while the on-state resistance decreased from 360 Ω.cm^2 at 25 °C to 30 Ω.cm^2 at 225 °C. The forward turn-on voltage was reduced from 4 V at 25 °C to 1.9 V at 225 °C. The reverse breakdown voltage at room temperature was ~4.2 kV, with a temperature coefficient of −16.5 V K^{-1}. This negative temperature coefficient precludes avalanche being the breakdown mechanism and indicates that defects still dominate the reverse conduction characteristics. The corresponding power figures-of-merit were 0.27–0.49 MW.cm^{-2}. The maximum on/off ratios improved with temperature from 2105 at 25 °C to 3 × 107 at 225 °C when switching from 5 V forward to 0 V. The high temperature performance of the NiO/β-(Al0.21Ga0.79)2O3/Ga2O3 lateral rectifiers is promising if the current rate of optimization continues.
 [DOI: 10.1149/2162-8777/ace6d6]

Manuscript submitted April 4, 2023; revised manuscript received June 23, 2023. Published July 21, 2023.

There is continued interest in β-Ga_2O_3 for power electronics due to the potential for significant power savings from the improved switching efficiency of such devices relative to lower bandgap semiconductors such as GaN and SiC.[1–3] This also translates to the possibility of higher temperature operation due to the lower intrinsic carrier concentration in Ga_2O_3. The increased electrification of automobiles and the need to efficiently switch renewable energy into power grids or to charge electric vehicles has increased interest in the use of ultra-wide bandgap semiconductors like Ga_2O_3 in power management and control systems.[4–23] This could lead to faster switching at higher power levels for more efficient charging systems and improved control and protection of power distribution systems.[22–30] Thus, the target is the realization of more efficient, high-power, high-speed electronic converters containing rectifiers and switches.[31–36]

The absence of shallow acceptor dopants in this material[4,5] has prompted the use of p-type oxides to form p–n junctions with n-type Ga_2O_3.[6,7] The most successful of these has been NiO, usually deposited by sputtering in which the O_2/Ar ratio can be used to control the conductivity.[8,9] The p-n junction has superior voltage blocking capability compared to Schottky rectifiers and ensures low leakage in the off state. The latter is advantageous for reliability and reduced power loss. The p–n junction also stops holes generated in the high field blocking region from accumulating in the bulk or at dielectric/semiconductor interfaces and also from being injected and trapped in the dielectrics. Lastly, a p–n junction enables non-destructive avalanche operation, which provides ruggedness for overvoltage situations. Many promising device results on vertical and lateral rectifiers using this heterojunction have been reported.[10–21] The NiO/β-Ga_2O_3 heterojunction has a type II band alignment,[9,37–39] which is retained up to annealing temperatures of at least 600 °C.[10] NiO has also been found to have a high critical field, in the range 5–10 MV.cm^{-1} [11] and has been employed for edge termination as well as p–n junction formation.[40,41] It has generally been deposited by sputtering but also can be grown epitaxially.[37,42]

While the characteristics of NiO/Ga_2O_3 rectifiers has been the focus, there is less information on their operation at elevated temperatures.[43,44] The temperature dependence of reverse recovery and on-off ratio on vertical NiO/Ga_2O_3 rectifiers showed a decrease in turn-on voltage and a reverse recovery time that was independent of temperature.[44] Hao et al.[41] reported reverse currents in vertical rectifier with NiO junction termination extension that increased significantly with temperature and was ascribed to trap-related leakage mechanisms such as Poole–Frenkel emission. They suggested the origin of the defects was sputtering damage and indeed thin damaged layers on NiO deposited Ga_2O_3 have been reported previously.[40] The use of epitaxially grown NiO should prevent this.[45] W-based contacts on Ga_2O_3 have proven stable to 500 °C,[42] while conventional Ni/Au contacts were operational to 325 °C.[44]

There are also advantages to replacing GaO_3 with $(Al_xGa_{1-x})_2O_3$ to improve breakdown voltage and power figure-of-merit.[23–25] The use of the alloy increases the barrier height of metals to this layer, which reduces reverse leakage current in vertical rectifiers, while grading the composition can mitigate increases in on-state resistance.[23] Masten et al.[22] used a similar approach to fabricate β-$(Al_xGa_{1-x})_2O_3$/β-Ga_2O_3 metal-semiconductor field effect transistors with promising performance. We have previously shown that such structures may reach high breakdown voltages, around 7 kV, but have relatively high on-resistance.[46]

In this paper, we report the temperature dependence of dc parameters for lateral NiO/β-$(Al_xGa_{1-x})_2O_3$/Ga_2O_3 heterojunction rectifiers grown by MOCVD with a bilayer NiO structure deposited by sputtering. The devices show promising temperature dependence of both on/off ratio and breakdown characteristics.

Experimental

The β-$(Al_xGa_{1-x})_2O_3$/β-Ga_2O_3 epitaxial structure was grown at low pressure (15 Torr) at 800 °C on a Fe doped (010) β-Ga_2O_3 1' substrate (Synoptics) in an Agnitron Agilis 500 multi-wafer MOCVD system. The precursors were trimethylaluminum (TMAl), triethylgallium (TEGa), and oxygen (5 N). The carrier gas was argon

*Electrochemical Society Student Member.
**Electrochemical Society Fellow.
zE-mail: hwan@ufl.edu

(6 N).[22,23] The layer structure is shown schematically in Fig. 1 top and consists of 70 nm thick Si doped β-$(Al_xGa_{1-x})_2O_3$ layer on ~300 nm UID β-Ga_2O_3 buffer. The AlGaO layer was doped with Si to 4×10^{17} cm^{-3} from a silane source diluted in nitrogen (SiH_4/N_2). The Al concentration in this layer was 20.6%, as determined by X-ray diffraction. The sheet resistance was7636 Ω sq^{-1}. and the sheet carrier concentration was 7.2×10^{12} cm^{-2}.[22] The electron mobility in the layer was 114 cm^2 $V{\cdot}s^{-1}$.

The NiO bilayer was deposited by rf magnetron sputtering at a working pressure of 3mTorr and 13.56 MHz. The gas flow ratio of Ar/O_2 was found to be the most important parameter in controlling the conductivity of the NiO. The bilayer NiO structure was used to optimize both sheet resistance and breakdown voltage. The large conduction band offset of NiO on AlGaO should lead to accumulation of electrons at the interface.[37,38] The NiO was contacted with 100 nm of Ni/Au, with circular contacts of 80 μm. The Ohmic contacts consisted of 100 nm of Ti/Au. As reported previously, the specific contact resistance was 0.12 Ω.cm^2, with a transfer length of 1.48 μm, while the sheet resistance under the Ti/Au Ohmic contact was 5.3×10^6 Ω $square^{-1}$. Note that no mesa etching is needed in this process. An optical image of the device layout is shown in Fig. 1(bottom).

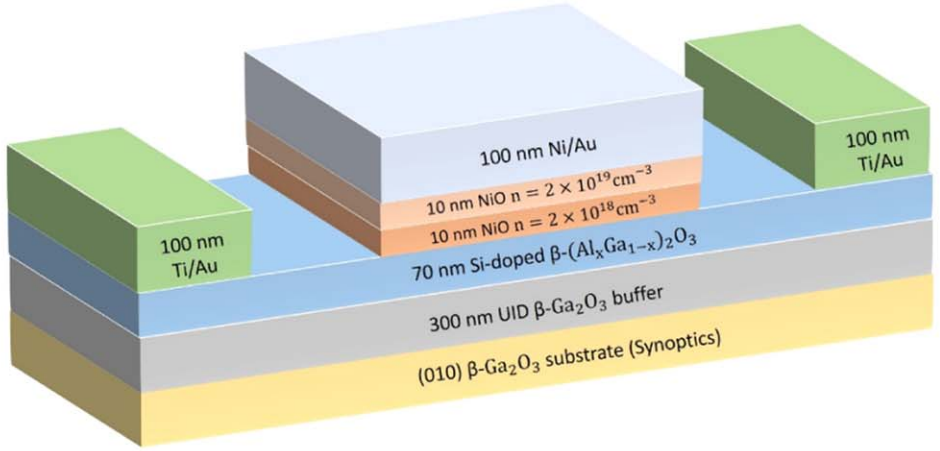

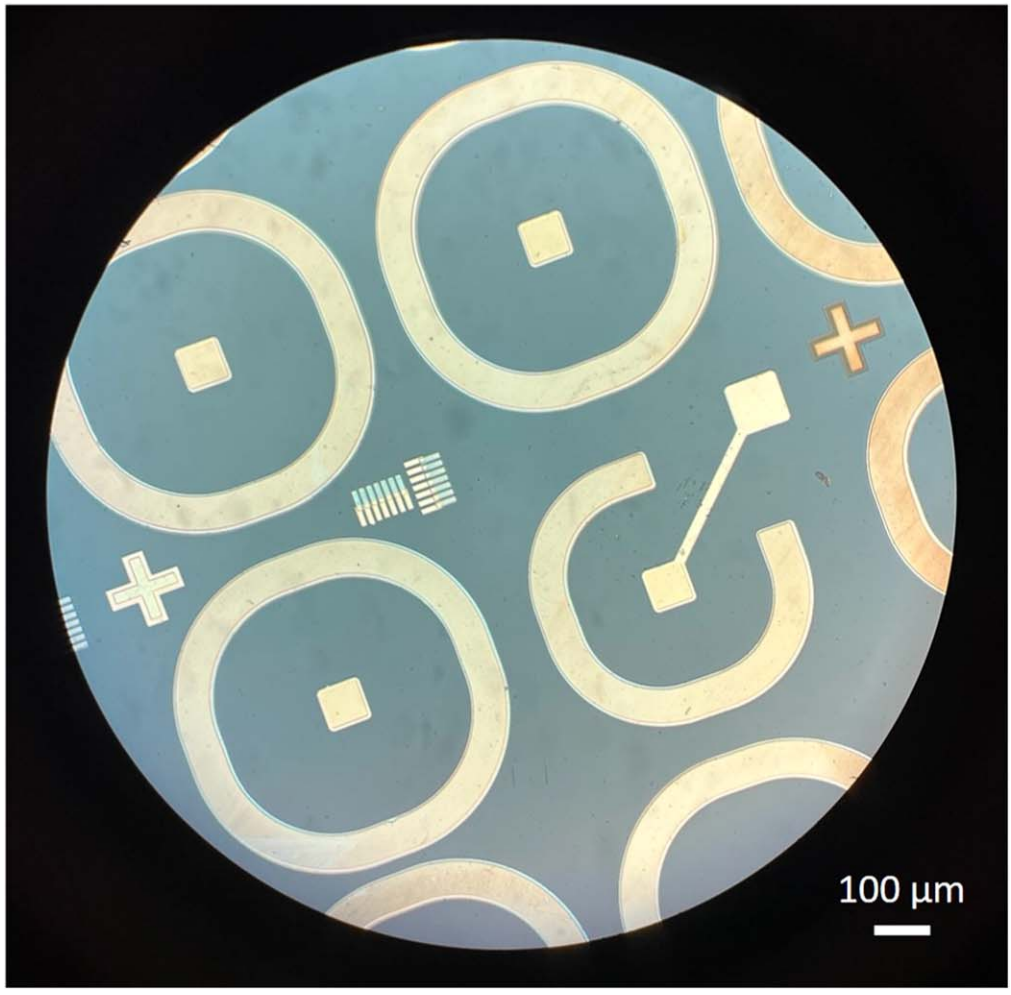

Figure 1. (Top) Schematic of lateral diode structure (bottom) optical image of completed devices.

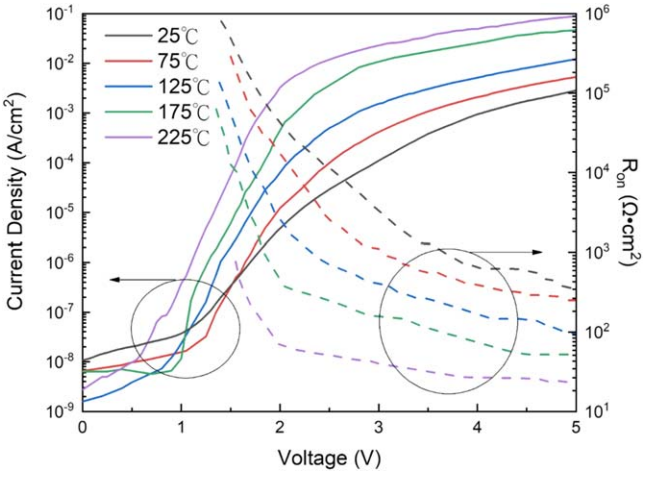

Figure 2. Forward current density and on-state resistance for rectifiers as a function of temperature.

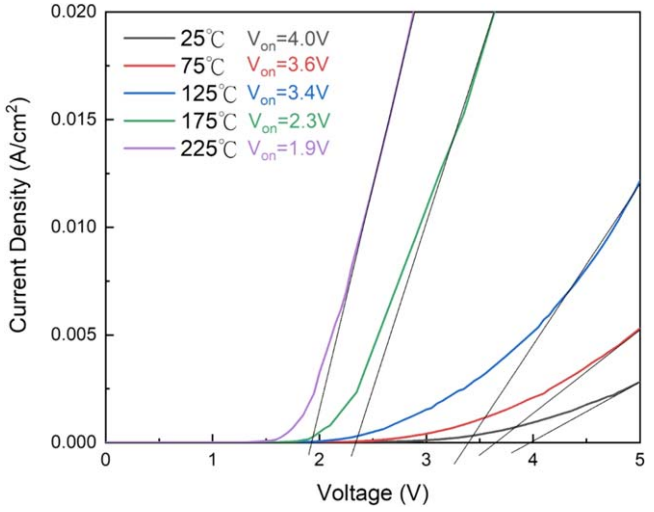

Figure 3. Linear J-V characteristics to extract forward turn-on voltage as a function of temperature.

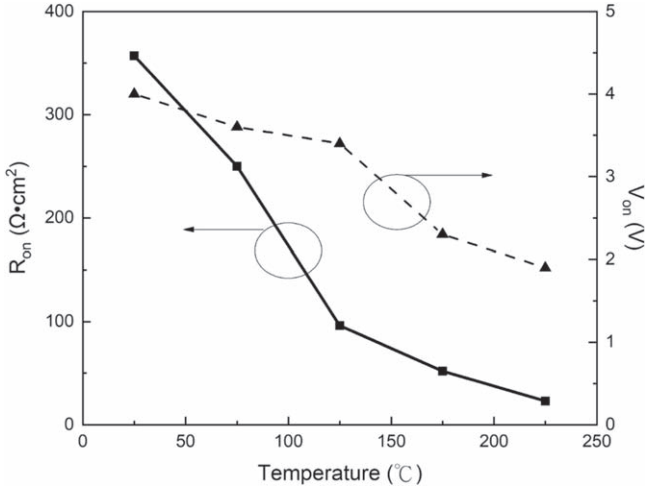

Figure 4. R_{ON} and V_{ON} as a function of temperature.

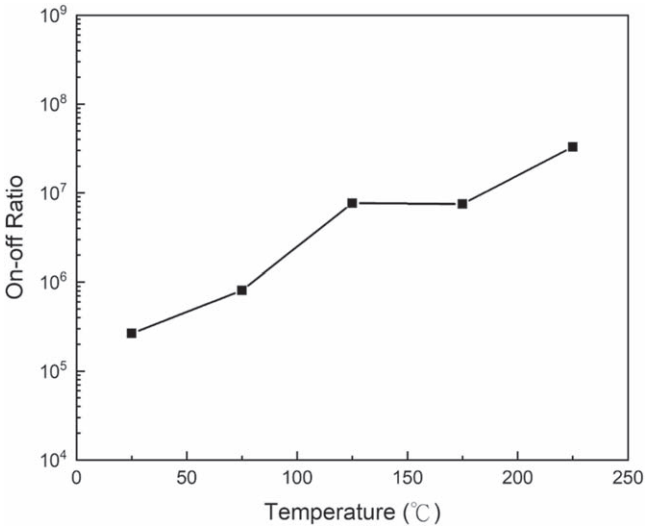

Figure 5. On/off ratio as a function of temperature when switching from +5 V to 100 V.

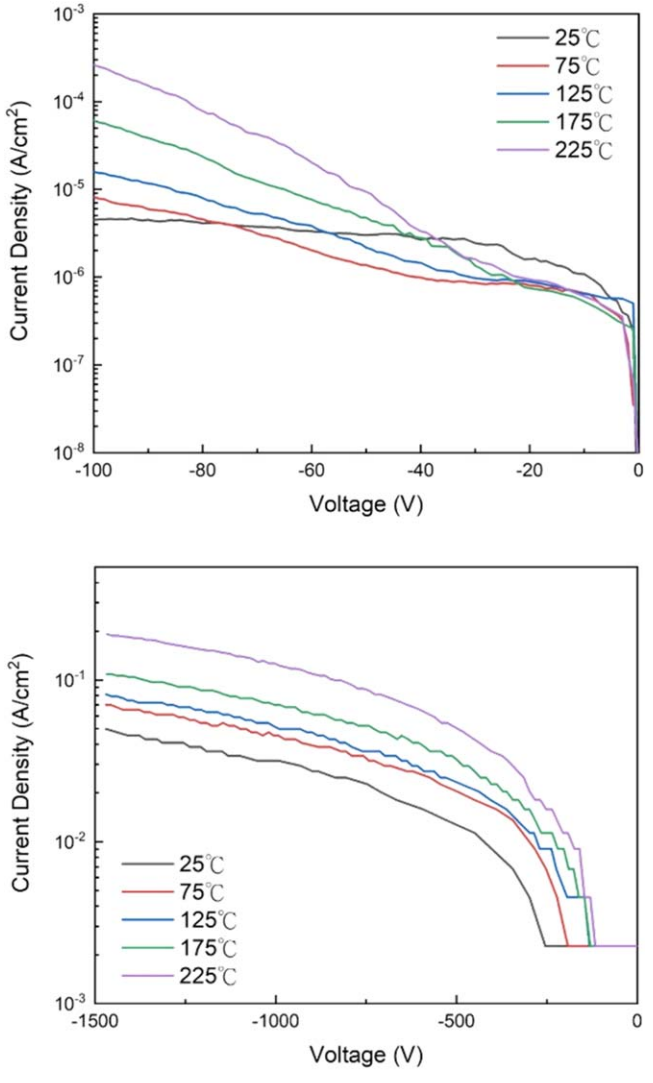

Figure 6. (Top) Reverse I–V characteristics of rectifiers up to (a) −100 V or (bottom) −1500 V as a function of temperature.

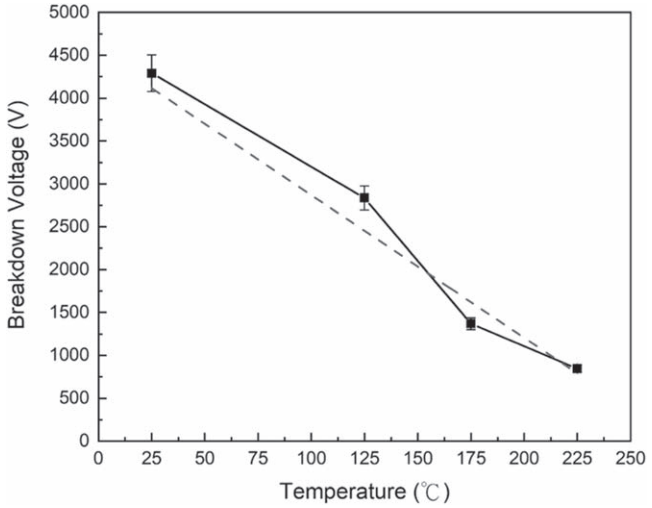

Figure 7. Temperature dependence of V_B.

The current density-voltage (J–V) characteristics from 25 °C–225 °C were measured on a Tektronix 371-B curve tracer at high voltage, while an Agilent 4156 C was used for forward and reverse current measurements at low biases. The reverse breakdown voltage was defined as the bias for a reverse current density reaching 0.1 A.cm^{-2}. The on-off ratio was measured over the same temperature range for switching from +5 V forward voltage to 0 V.

Results and Discussion

Figure 2 shows the forward current density characteristics and on-state resistances, R_{ON}, for temperatures from 25 °C–225 °C. The forward current increases with temperature, indicating the effective barrier height is strongly temperature dependent. This indicates the forward characteristic deviates from ideal thermionic emission. Often this is a result of inhomogeneity of the interface under the Ni/Au contacts.[47] These J–V characteristics are linear at low biases, while deviating from linearity at higher voltage due to series resistance effects. The R_{ON} values ranged from 360 Ω.cm^2 at 25 °C to 30 Ω.cm^2 at 225 °C.

The same data is shown in linear form in Fig. 3, allowing the turn-on voltage to be obtained from the intercept of each plot. These were reduced from 4 V at 25 °C to 1.9 V at 225 °C. This is an advantage for these devices in terms of operating at elevated temperatures, as the forward conduction begins at lower voltages.

The temperature dependence of R_{ON} and V_{ON} is shown in Fig. 4. Note that R_{ON} shows a monotonic decrease over the entire temperature range examined, showing the expected decrease in carrier mobility at elevated temperatures is outweighed by the decrease in effective barrier height and bandgap.

Figure 5 shows the temperature dependence of the on-off ratio, which improved with temperature from 2×10^5 at 25 °C to 3×10^7 at 225 °C when switching from 5 V forward to 0 V. This is also an advantage for elevated temperature operation of these lateral rectifiers.

The reverse J–V characteristics are shown for low bias up to −100 V in Fig. 6 (top) and for larger biases (1500 V) in Fig. 6 (bottom). This reverse leakage current was dominated by thermionic field emission in the low bias range, while at higher biases, the dominant transport mechanism is trap-assisted space-charge-limited conduction. The breakdown voltages as a function of temperature were extracted from the reverse J–V characteristics, as shown in Fig. 7. The breakdown at 25 °C was ∼4.2 kV, with a temperature coefficient of −16.5 V K^{-1}. This negative temperature coefficient shows that the breakdown is not due to the avalanche breakdown mechanism since that should exhibit a positive temperature coefficient.[45] Our experimental data for V_B with temperature can be expressed as:

$$V_B = V_{B0}\,1 + \beta(T - T_0)$$

where $\beta = -16.5 \pm 1.6$ V. K^{-1}. Previous work has shown in vertical geometry Ga_2O_3 rectifiers that impact ionization of deep acceptors is a strong contributor to breakdown, but those samples were grown by hydride vapor phase epitaxy and would not necessarily have the same impurities as these more refined MOCVD grown layers. For comparison, room temperature breakdown voltages in Ga_2O_3 metal semiconductor MESFETs and MOSFETs are typically 2–4 kV.[48–54] The highest breakdown voltage for a lateral MOSFET is 8.56 kV in vacuum annealed devices,[45,52] although the performance as a function of temperature was not reported.

The power figure-of-merit (FOM), V_B^2/R_{ON}, where V_B is the reverse breakdown voltage, for the rectifiers was in the range 0.27–0.49 MW.cm^{-2} over our investigated temperature range.

The breakdown fields calculated from the observed breakdown voltages at different temperatures were 5.25×10^5 V cm^{-1} at 25 °C, and 1.2×10^5 V cm^{-1} at 225 °C. Currently, all Ga_2O_3 lateral as well as vertical rectifiers show performance limited by the presence of defects and by breakdown initiated in the depletion region near the electrode corners.

Since inverter systems need both switching devices and rectifiers, lateral geometry devices in this ultra-wide bandgap materials system are also of interest. Since a key goal in enhancing the efficiency and resilience of power grids is to enable faster switching and/or triggering at higher current and voltage levels, for Ga_2O_3 to play a role, the on-state resistance must be reduced while retaining the high breakdown voltages. Note that all of the reported figures of merit for lateral devices still fall well short of the theoretical values for Ga_2O_3, with only some being superior at this stage to the limits for Si. This emphasizes how much more development is needed for Ga_2O_3 power electronics.

Summary and Conclusions

The performance of NiO/β-$(Al_{0.21}\ Ga_{0.79})_2O_3$/$Ga_2O_3$ heterojunction lateral geometry rectifiers was studied for temperatures up to 225 °C. While the rectifiers show a negative temperature coefficient for breakdown voltage, both R_{ON} and V_{ON} decrease with temperature. Positive temperature coefficients would indicate that the breakdown in the diodes is being determined by avalanche breakdown caused by impact ionization. The dominant breakdown mechanism in Ga_2O_3 devices is not yet clear and it is not obvious that classical avalanche (impact ionization) occurs in such a wide bandgap material with a significant degree of ionicity in its bonds. Differences in electronic structure could lead to other dielectric breakdown processes, such as bond breakage and material degradation and/or electron emission. For instance, the ionization coefficient of electrons in Ga_2O_3 is much lower than that of holes, since the width of the lowest-lying conduction band is narrower than the bandgap itself. In addition, the electron affinity is smaller than the bandgap. In current Ga_2O_3 devices there is clear evidence that breakdown occurs by tunneling or direct impact ionization of trap states.

In addition, previous work has shown the $(Al_{0.21}\ Ga_{0.79})_2O_3$ and NiO are both thermally stable above this temperature. The high R_{ON} values mean the device performance is far from the AlGaO limit, with the R_{ON} values inferior to the projected Si limit. This is an area that must be optimized. The use of the industry standard MOCVD growth, simple fabrication and avoidance of mesa etching processes are all advantages of the approach outlined in this work. There is still room for further improvement in breakdown voltage by field plates and other edge termination methods. Recent progress in extending the breakdown voltage above 8 kV in vertical rectifiers has shown the value of field management.[55–57]

Acknowledgments

Work performed as part of Interaction of Ionizing Radiation with Matter University Research Alliance (IIRM-URA),

sponsored by the Department of the Defense, Defense Threat Reduction Agency under award HDTRA1–20–2–0002. The content of the information does not necessarily reflect the position or the policy of the federal government, and no official endorsement should be inferred. The work was also supported by NSF DMR 1856662. The authors thank the staff of the Nanoscale Research Facility at UF, part of the Herbert Wertheim College of Engineering's Research Service Centers (RSC) for assistance in device fabrication. H.N.M. and J.S.L acknowledge postdoctoral funding from the National Research Council, Washington DC. Fabrication equipment and support was provided by the NRL Nanoscience Institute and Dr. Brian Downey (NRL). The authors acknowledge Dr. John Blevins (AFRL) for providing Ga_2O_3 substrates for this work. Agnitron's ongoing β-Ga_2O_3 development work is in part supported by ONR contract number N6833518C0192, under the direction of Mr Lynn Petersen. Research at the Naval Research Laboratory was supported by the Office of Naval Research.

Data Availability

The data that supports the findings of this study are available within the article.

ORCID

Hsiao-Hsuan Wan https://orcid.org/0000-0002-6986-8217
Jian-Sian Li https://orcid.org/0000-0002-2817-7612
Chao-Ching Chiang https://orcid.org/0000-0002-0447-8170
Xinyi Xia https://orcid.org/0000-0002-8644-8599
S. J. Pearton https://orcid.org/0000-0001-6498-1256

References

1. M. Tadjer, *Science*, **378**, 6621 (2022).
2. S. J. Pearton, J. Yang, P. H. Cary IV, F. Ren, J. Kim, M. J. Tadjer, and M. A. Mastro, *Appl. Phys. Rev.*, **5**, 011301 (2018).
3. P. Dong, J. Zhang, Q. Yan, Z. Liu, P. Ma, H. Zhou, and Y. Hao, *IEEE Electron Dev Lett.*, **43**, 765 (2022).
4. E. Chikoidze et al., *J. Mater. Chem.*, **C7**, 10231 (2019).
5. A. Kyrtsos, M. Matsubara, and E. Bellotti, *Appl. Phys. Lett.*, **112**, 032108 (2018).
6. Y. Kokubun, S. Kubo, and S. Nakagomi, *Appl. Phys. Express*, **9**, 091101 (2016).
7. S. Nakagomi, T. T. Yasuda, and Y. Kokubun, *Phys. Status Solidi b*, **257**, 1900669 (2020).
8. X. Xia, J. S. Li, C. C. Chiang, F. Ren, and S. J. Pearton, *J. Vac. Sci. Technol. A*, **41**, 013405 (2022).
9. X. Xia, J. S. Li, C. C. Chiang, T. J. Yoo, F. Ren, H. Kim, and S. J. Pearton, *J. Phys. D: Appl. Phys.*, **55**, 385105 (2022).
10. W. Hao, Q. He, K. Zhou, G. Xu, W. Xiong, X. Zhou, G. Jian, C. Chen, X. Zhao, and S. Long, *Appl. Phys. Lett.*, **118**, 043501 (2021).
11. Y. Wang et al., *IEEE Trans. Power Electron.*, **37**, 3743 (2022).
12. K. S. Danno, M. Kado, T. Hara, T. Takasugi, H. Yamano, Y. Umetani, and T. Shoji, *Jpn. J. Appl. Phys.*, **62**, SF1007 (2023).
13. E. Ahmadi and Y. Oshima, *J. Appl. Phys.*, **126**, 160901 (2019).
14. S. J. Pearton, F. Ren, M. Tadjer, and J. Kim, *J. Appl. Phys.*, **124**, 222901 (2018).
15. J. Zhang et al., *Nat. Commun.*, **13**, 3900 (2022).
16. T. Watahiki, Y. Yuda, A. Furukawa, M. Yamamuka, Y. Takiguchi, and S. Miyajima, *Appl. Phys. Lett.*, **111**, 222104 (2017).
17. J. Zhang, S. Han, M. Cui, X. Xu, W. Li, H. Xu, C. Jin, M. Gu, L. Chen, and K. H. L. Zhang, *ACS Appl. Electron. Mater.*, **2**, 456 (2020).
18. Y. Lv et al., *IEEE Trans. Power Electron.*, **36**, 6179 (2021).
19. H. H. Gong, X. H. Chen, Y. Xu, F.-F. Ren, S. L. Gu, and J. D. Ye, *Appl. Phys. Lett.*, **117**, 022104 (2020).
20. F. Zhou et al., *IEEE Trans. Power Electron.*, **37**, 1223 (2022).
21. J.-S. Li, C.-C. Chiang, X. Xia, F. Ren, H. Kim, and S. J. Pearton, *Appl. Phys. Lett.*, **121**, 042105 (2022).
22. H. N. Masten, J. S. Lundh, J. A. Spencer, F. Alema, A. Osinsky, A. G. Jacobs, K. D. Hobart, and M. J. Tadjer, "Demonstration of MOCVD Si-doped β-$(Al_xGa_{1-x})_2O_3$ Recessed-Gate MESFET." *Presented at IWGO 2022* (Japan, Nagano) (2022), https://iwgo2022.org/index.php/about-this-workshop/.
23. P. P. Sundaram, F. Alema, A. Osinsky, and S. J. Koester, *J. Vac. Sci. Technol. A*, **40**, 043211 (2022).
24. D. H. Mudiyanselage, D. Wang, and H. Fu, *J. Vac. Sci. Technol. A*, **41**, 023201 (2023).
25. A. F. M. A. U. Bhuiyan, Z. Feng, H. Huang, L. Meng, J. Hwang, and H. Zhao, *J. Vac. Sci. Technol. A*, **39**, 063207 (2021).
26. G. Seryogin, F. Alema, N. Valente, H. Fu, E. Steinbrunner, A. T. Neal, S. Mou, A. Fine, and A. Osinsky, *Appl. Phys. Lett.*, **117**, 262101 (2020).
27. K. Konishi, K. Goto, H. Murakami, Y. Kumagai, A. Kuramata, S. Yamakoshi, and M. Higashiwaki, *Appl. Phys. Lett.*, **110**, 103506 (2017).
28. K. Sasaki, D. Wakimoto, Q. T. Thieu, Y. Koishikawa, A. Kuramata, M. Higashiwaki, and S. Yamakoshi, *IEEE Electron Dev Lett.*, **38**, 783 (2017).
29. J. Yang, F. Ren, M. Tadjer, S. J. Pearton, and A. Kuramata, *ECS J. Solid State Sci. Technol.*, **7**, Q92 (2018).
30. J. Yang, F. Ren, Y. T. Chen, Y. T. Liao, C. W. Chang, J. Lin, M. J. Tadjer, S. J. Pearton, and A. Kuramata, *IEEE J. Electron Dev.*, **7**, 57 (2019).
31. Z. Hu, H. Zhou, K. Dang, Y. Z. Cai Feng, Y. Gao, Q. Feng, J. Zhang, and Y. Hao, *IEEE J. Electron Dev.*, **6**, 815 (2018).
32. C. Joishi, S. Rafique, Z. Xia, L. Han, S. Krishnamoorthy, Y. Zhang, S. Lodha, H. Zhao, and S. Rajan, *Appl. Phys. Express*, **11**, 031101 (2018).
33. W. Li, K. Nomoto, Z. Hu, D. Jena, and H. G. Xing, *IEEE Electron. Dev Lett.*, **41**, 107 (2020).
34. M. Ji, N. R. Taylo, I. Kravchenko, P. Joshi, T. Aytug, L. R. Cao, and M. Parans Paranthaman, *IEEE Trans. Power Electron.*, **36**, 41 (2021).
35. M. Xiao et al., *IEEE Trans. Power Electron.*, **36**, 8565 (2021).
36. W. Xiong et al., *IEEE Electron Dev Lett.*, **42**, 430 (2021).
37. J. A. Spencer, A. L. Mock, A. G. Jacobs, M. Schubert, Y. Zhang, and M. J. Tadjer, *Appl. Phys. Rev.*, **9**, 011315 (2022).
38. X. Lu, X. Zhou, H. Jiang, K. W. Ng, Z. Chen, Y. Pei, K. M. Lau, and G. Wang, *IEEE Electron Dev Lett.*, **41**, 449 (2020).
39. H. Gong, X. Chen, Y. Xu, Y. Chen, F. Ren, B. Liu, S. Gu, R. Zhang, and J. Ye, *IEEE Trans Electron Dev.*, **67**, 3341 (2020).
40. J. S. Li, C. C. Chiang, X. Xia, T. Yoo, F. Ren, H. Kim, and S. J. Pearton, *J. Vac. Sci. Technol. A*, **40**, 063407 (2022).
41. W. Hao et al., *IEEE Trans Electron Dev*, **70**, 2129 (2023).
42. K. Uchida, K.-ichi Yoshida, D. Zhang, A. Koizumi, and S. Nozaki, *AIP Adv.*, **2**, 042154 (2012).
43. C. Fares, F. Ren, and S. J. Pearton, *ECS J. Solid State Sci. Technol.*, **8**, Q3007 (2019).
44. X. Xia, M. Xian, P. Carey, C. Fares, F. Ren, M. Tadjer, S. J. Pearton, T. Q. Tu, K. Goto, and A. Kuramata, *J. Phys. D*, **54**, 305103 (2021).
45. K. Zeng, S. Chowdhury, B. Gunning, R. Kaplar, and T. Anderson, "Study on avalanche uniformity in 1.2 KV GaN Vertical PIN Diode with bevel edge-termination." *2021 IEEE International Reliability Physics Symposium (IRPS)*, Monterey, CA, USA, p. 1 (2021).
46. H. H. Wan et al., *J. Vac. Sci. Technol. A*, **41**, 032701 (2023).
47. H. Sheoran, B. R. Tak, N. Manikanthababu, and R. Singh, *ECS J. Solid State Sci. Technol.*, **9**, 055004 (2020).
48. A. Bhattacharyya, S. Sharma, F. Alema, P. Ranga, S. Roy, C. Peterson, G. Seryogin, A. Osinsky, U. Singisetti, and S. Krishnamoorthy, *Appl. Phys. Express*, **15**, 061001 (2022).
49. Y. Lv et al., *IEEE Electron Dev Lett.*, **41**, 537 (2020).
50. A. Bhattacharyya, P. Ranga, S. Roy, C. Peterson, F. Alema, G. Seryogin, A. Osinsky, and S. Krishnamoorthy, *IEEE Electron Dev Lett.*, **42**, 1272 (2021).
51. K. Zeng, A. Vaidya, and U. Singisetti, *IEEE Electron Dev Lett.*, **39**, 1385 (2018).
52. K. Tetzner, E. Bahat Treidel, O. Hilt, A. Popp, S. Bin Anooz, G. Wagner, A. Thies, K. Ickert, H. Gargouri, and J. Würf, *IEEE Electron Dev. Lett.*, **40**, 1503 (2019).
53. S. Sharma, L. Meng, A. F. M. Anhar Uddin Bhuiyan, Z. Feng, D. Eason, H. Zhao, and U. Singisetti, *IEEE Electron Dev Lett*, **43**, 2029 (2022).
54. S. Sharma, K. Zeng, S. Saha, and U. Singisetti, *IEEE Electron Dev Lett.*, **41**, 836 (2020).
55. J. S. Li, C. C. Chiang, X. Xia, H. H. Wan, F. Ren, and S. J. Pearton, *J. Mater. Chem. C*, **11**, 7750 (2023).
56. J. S. Li, H. H. Wan, C. C. Chiang, X. Xia, T. Yoo, H. Kim, F. Ren, and S. J. Pearton, *Crystals*, **13**, 886 (2023).
57. J. S. Li, C. C. Chiang, X. Xia, H. H. Wan, F. Ren, and S. J. Pearton, *J. Vac. Sci. Technol. A*, **41**, 043404 (2023).